State-Feedback Control of Longitudinal Combustion Instabilities

Vigor Yang,* Alok Sinha,* and Youn-Tih Fung†
Pennsylvania State University, University Park, Pennsylvania 16802

Active control of longitudinal pressure oscillations in combustion chambers has been studied theoretically by means of a digital state-feedback control technique. The formulation is based on a generalized wave equation that accommodates all influences of combustion, mean flow, unsteady motions, and control actions. Following a procedure equivalent to the Galerkin method, a system of ordinary differential equations governing the amplitude of each oscillatory mode is derived for the controller design. The control actions are provided by a finite number of point actuators, with instantaneous chamber conditions monitored by multiple sensors. Several important control aspects, including sampling period, locations of sensors and actuators, controllability, and observability, have been investigated systematically. As a specific example, the case involving two controlled and two residual (uncontrolled) modes is studied.

Nomenclature

A = continuous-time system matrix
$\bar{a}$ = speed of sound in mixture
B = continuous-time input matrix
C = output matrix
$\mathcal{C}$ = controllability matrix
D_{ni} = linear parameters, Eq. (16)
E_{ni} = linear parameters, Eq. (16)
e_N = estimation error
F = discrete-time system matrix
f = source terms for boundary conditions
G = discrete-time input matrix
h = source terms in wave equation
J = objective function, Eq. (44)
K = number of total modes
$\mathcal{K}$ = system-feedback gain matrix
k_n = wave number
L = length of combustion chamber
$\mathcal{L}$ = estimator-feedback gain matrix
M = number of actuators
N = number of controlled modes
$\mathcal{O}$ = observability matrix
P = number of sensors
R = number of residual modes
T_S = sampling period
U_n = control input of nth mode
$\boldsymbol{u}$ = control input vector
v_n = measurement noise of nth mode
W = weighting factor
w_n = system noise of nth mode
$\boldsymbol{x}$ = state variables
$\boldsymbol{y}$ = sensor output vector
z_a = position of sensor or actuator
$\bar{\alpha}_i$ = coefficient of system characteristic polynomial
$\bar{\beta}_i$ = coefficient of observer characteristic polynomial
η_n = amplitude of nth mode
$\bar{\gamma}$ = specific heat ratio of mixture
ψ_n = normal mode shape of nth mode
ω_n = normal frequency of nth mode

Subscripts

c = control input
N = controlled mode
R = residual mode
0 = initial values

Superscripts

$\dot{(\,)}$ = time derivative
$\bar{(\,)}$ = mean quantity
$\hat{(\,)}$ = estimated state
$(\,)'$ = fluctuation

Introduction

THE desire to advance propulsion technology has led to efforts to control and optimize various operating characteristics of combustion systems. Principal among these is the moderation or control of pressure oscillations (generically known as combustion instabilities) in combustion chambers. Heat released by combustion is the source of energy that sustains such oscillations. There appears to be little doubt that the most intense motions owe their existence to the mutual coupling between unsteady combustion response and periodic flow oscillations. As a result, the oscillations appear as the motions of a self-excited system. The ensuing structural vibration and thrust variation may significantly compromise the overall system performance.

Many attempts have been made to overcome combustion instability problems or to prevent their occurrence. These efforts usually fall into two categories: 1) making changes in the system designs so that the coupling between combustion response and unsteady wave motions can be minimized; and 2) making changes in dynamic energy losses so that they exceed the energy gains from the combustion response.[1] Although the effectiveness of these methods has been demonstrated in certain situations, a number of fundamental problems remain unresolved. First, most existing techniques are static in nature and are based on passive means. The instability suppression mechanisms operate only for a narrow frequency range and do not respond effectively to spatial and temporal variations of flow conditions. Second, no unified theories have been constructed for the optimization of the control device. The entire system was developed primarily on a trial-and-error basis. The experience gained from one system may not be directly applicable to other systems. Third, and perhaps most important, for many practical systems there is no passive means available to control instabilities.

Although traditional passive control techniques need improvement and further optimization, a new technology based on active instability control (AIC) offers radically new solu-

Received Dec. 16, 1988; revision received April 19, 1990; accepted for publication April 23, 1990.

*Associate Professor, Department of Mechanical Engineering. Member AIAA.
†Graduate Student, Department of Mechanical Engineering.

tions, particularly in the regime where passive control techniques are ineffective, impractical, too costly, or have reached their design limits. The AIC methods incorporate modern control theories and offer capabilities of estimating instantaneous flow conditions, calculating optimal control feedback gains, and exerting control actions on the flowfields. Figure 1 presents a schematic of the proposed system. Important physical variables in the combustor are monitored by appropriate sensors at representative positions. The measured signals are then filtered and processed by a microprocessor in which the suitable control inputs are calculated instantaneously according to a predescribed model. Finally, the control inputs are applied to modify the flow conditions. If designed properly, the system may attenuate undesired oscillations within a few cycles. Recent works on the active control of thermoacoustic oscillations[2–8] have demonstrated clearly the advantages of this technique.

The purpose of this paper is to provide a theoretical framework for designing an active control system for the suppression of combustion instabilities. In what follows, a general analysis of unsteady motions in a combustion chamber is given, followed by a comprehensive discussion of the controller design. As a specific example, the case involving a finite number of controlled and residual modes is addressed in detail.

Formulation

The formulation extends the previous analyses for nonlinear combustion instabilities[9,10] and accommodates actively controlled external forcing functions. To concentrate on the construction of active control algorithms, we restrict the following discussion to the thermoacoustic oscillations in a combustion chamber. The problem involving shear layer or vortical instabilities will be treated elsewhere. In brief, we assume that the medium in the chamber consists of a two-phase mixture. The gas phase contains inert species, reactants, and combustion products. The liquid phase is composed of fuel and/or oxidizer droplets, and is treated as a fluid with density ρ_ℓ, mass per unit volume of the chamber. Conversion of liquid phases to gas may occur at the rate $\bar{\omega}_\ell$ due to droplet vaporization or combustion. Its unsteady behavior can be correctly modeled as a distribution of time-varying mass, momentum, and energy perturbations to the gas-phase flowfield. If the droplets are taken to be dispersed, the conservation equations for a two-phase mixture can be written in the following form, involving the mass-averaged properties of the flow,

$$\frac{\partial \rho}{\partial t} + v_g \cdot \nabla \rho = \mathcal{W} \tag{1}$$

$$\rho \frac{\partial v_g}{\partial t} + \rho v_g \cdot \nabla v_g = -\nabla p + \mathcal{F} \tag{2}$$

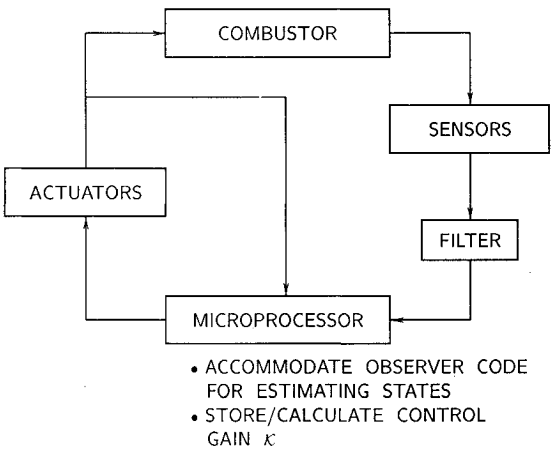

Fig. 1 Schematic diagram of active control of combustion instabilities.

$$\frac{\partial p}{\partial t} + \bar{\gamma} p \nabla \cdot v_g = -v_g \cdot \nabla p + \mathcal{P} \tag{3}$$

where

$$\mathcal{W} = -\rho \nabla \cdot v_g - \nabla \cdot (\rho_\ell \delta v_\ell) \tag{4}$$

$$\mathcal{F} = \nabla \cdot \tau_v + \delta F_\ell + \delta v_\ell \bar{\omega}_\ell \tag{5}$$

$$\mathcal{P} = (\bar{R}/\bar{C}_v)[Q + \delta Q_\ell + \nabla \cdot q + \delta v_\ell \cdot F_\ell + \{(h_\ell - e_g) + \tfrac{1}{2}(\delta v_\ell)^2\}\bar{\omega}_\ell - \bar{C}_v T_g \nabla \cdot (\rho_\ell \delta v_\ell)] \tag{6}$$

and $\delta v_\ell = v_\ell - v_g$, $\delta h_\ell = h_\ell - C_\ell T$. The subscripts g and ℓ stand for the mass-averaged quantities for gas and liquid phases, respectively, and ρ is the density of the mixture. The viscous stress tensor and conductive heat flux vector are represented respectively by τ_v and q; Q is the energy released by homogeneous reactions in the gas phase. The force of interaction and energy transfer between gas and liquid are δF_ℓ and δQ_ℓ, respectively.

To control combustion instabilities, we may exert appropriate external influence on the unsteady mass, momentum, and energy in the chamber. Whatever physical means are devised, control inputs must be theoretically treated as sources in the conservation equations and their subsequent forms. Therefore, Eqs. (1–3) are modified by adding control inputs $\mathcal{W}_c$, $\mathcal{F}_c$, and $\mathcal{P}_c$ on the right-hand sides. Their specific details depend on the kind of control implemented, and are less important here in developing a general framework.

A wave equation governing the unsteady motions is then derived by decomposition of the dependent variables into mean and time-dependent quantities. To simplify matters, variations are ignored in the mean pressure, temperature, and density, but the mean flow velocity is both nonzero and nonuniform. This amounts to assuming that the mean Mach number is relatively small, a situation commonly found in practice. However, there may be circumstances in which changes of mean values are important; to accommodate these requires considerable elaboration not justified here. Thus,

$$\rho = \bar{\rho} + \rho'(r,t) \tag{7a}$$

$$v_g = \bar{v}_g(r) + v_g'(r,t) \tag{7b}$$

$$p = \bar{p} + p'(r,t) \tag{7c}$$

Since combustion instabilities manifest themselves by the presence of pressure oscillations, and pressure signals can be measured directly and processed at sufficiently high frequencies, the wave equation can be most conveniently written in terms of pressure. Now substitute Eqs. (7) in Eqs. (1–3), collect coefficients of like powers, and rearrange the results to obtain the following wave equation:

$$\nabla^2 p' - \frac{1}{\bar{a}^2}\frac{\partial^2 p'}{\partial t^2} = h + h_c \tag{8}$$

Boundary conditions are found by first taking the scalar product of the outward normal vector with the perturbed momentum Eq. (2), and then using appropriate acoustic admittance functions along the surface of the chamber:

$$n \cdot \nabla p' = -f - f_c \tag{9}$$

where h_c and f_c represent the influences associated with the control inputs and are shown to be

$$h_c = \nabla \cdot \mathcal{F}_c' - \frac{1}{\bar{a}^2}\frac{\partial \mathcal{P}_c'}{\partial t} \tag{10a}$$

$$f_c = -n \cdot \mathcal{F}_c' \tag{10b}$$

The functions h and f contain all linear and nonlinear processes of acoustic motions, mean flow, and combustion, under conditions with no external forcing. Their explicit expressions are

$$h = -\bar{\rho}\nabla\cdot(\bar{v}_g\cdot\nabla v_g' + v_g'\cdot\nabla\bar{v}_g) + \frac{1}{\bar{a}^2}\bar{v}_g\cdot\nabla\frac{\partial p'}{\partial t} + \frac{\bar{\gamma}}{\bar{a}^2}\frac{\partial p'}{\partial t}\nabla\cdot v_g - \nabla\cdot\left(\bar{\rho}v_g'\cdot\nabla v_g' + \rho'\frac{\partial v_g'}{\partial t}\right) + \frac{1}{\bar{a}^2}\frac{\partial}{\partial t}(v_g'\cdot\nabla p') + \frac{\bar{\gamma}}{\bar{a}^2}\frac{\partial}{\partial t}(p'\nabla\cdot v_g') + \nabla\cdot\mathfrak{F}' - \frac{1}{\bar{a}^2}\frac{\partial\mathcal{Q}'}{\partial t} \tag{11a}$$

$$f = \bar{\rho}\frac{\partial v_g'}{\partial t}\cdot n + \bar{\rho}(\bar{v}_g\cdot\nabla v_g' + v_g'\cdot\nabla\bar{v}_g)\cdot n + \bar{\rho}(v_g'\cdot\nabla v_g')\cdot n + \rho'\frac{\partial v_g'}{\partial t}\cdot n - \mathfrak{F}'\cdot n \tag{11b}$$

To simplify the design of a feedback control system, the external forcing is assumed to be provided by M point actuators; each actuator supplies acoustic pressure excitation $u_i(t)$ at a predetermined position r_i. Accordingly, h_c takes the form

$$h_c(r,t) = \sum_{i=1}^{M}\delta(r - r_i)u_i(t) \tag{12}$$

where $\delta(r - r_i)$ is the Dirac delta function. Representation of the control source by the point actuator is justified when the acoustic wavelength is long compared to the actuator dimension, a criterion usually met for low-frequency oscillations. For problems in which the control source is not compact, extension of the analysis must be made to accommodate distributed actuators.[11]

If the mean Mach number is small, the source terms in Eqs. (8) and (9) can be treated as perturbations to the system. In the limiting case, where all perturbations vanish ($h = h_c = f = f_c = 0$), the wave equation for the pressure in classical acoustics with the boundary condition for a rigid wall is recovered. We may take advantage of this observation by approximating the solution of the wave equation, Eq. (8), with a synthesis of the normal modes:

$$p'(r,t) = \bar{p}\sum_{n=1}^{K}\eta_n(t)\psi_n(r) \tag{13a}$$

$$v'(r,t) = \sum_{n=1}^{K}\frac{\dot{\eta}_n(t)}{\bar{\gamma}k_n^2}\nabla\psi_n(r) \tag{13b}$$

where the normal mode function ψ_n satisfies the equation

$$\nabla^2\psi_n + k_n^2\psi_n = 0 \tag{14a}$$

with

$$n\cdot\nabla\psi_n = 0 \tag{14b}$$

along the boundary. For longitudinal pressure oscillations in a uniform chamber,

$$\psi_n = \cos\frac{n\pi}{L}z \tag{15}$$

Thus, the unsteady motions have structures closely related to those of the classical acoustic modes for a chamber closed at both ends, but with unknown time-varying amplitudes. This appears to be the most common situation in practical propulsion systems. It is worth noting that selection of appropriate normal mode functions depends intimately on the geometry of the chamber and the boundary conditions associated with the physical problem in question. For example, the boundary conditions for a chamber having two open ends (such as a Rijke tube) require that the unsteady pressure be zero at both ends. Therefore, the appropriate mode function ψ_n for that case is $\sin(n\pi z/L)$.

Theoretically, the system requires an infinite number of modes ($K\to\infty$) to complete the description of its behavior. In practice, however, the unsteady motions can be represented with fidelity by a truncated modal expansion, Eqs. (13), in which K may be large but still finite. This approximation is justified by the fact that high-frequency oscillations can be efficiently damped out by increased viscous dissipation, and may not actually exist physically. After substitution of Eqs. (13) into Eq. (8), and with the aid of spatial averaging, a set of ordinary differential equations is obtained for the time-dependent amplitude of each mode,[9,10]

$$\ddot{\eta}_n + \omega_n^2\eta_n + \sum_{i=1}^{K}(D_{ni}\dot{\eta}_i + E_{ni}\eta_i) + F_n^{NL}(\eta_1, \eta_2, \ldots, \dot{\eta}_1, \dot{\eta}_2, \ldots) = w_n(t) + U_n(t), \qquad n = 1,2,\ldots,K \tag{16}$$

where $w_n(t)$ is the system noise. D_{ni} and E_{ni} are linear coefficients associated with growth rate and frequency shift, respectively. The function F_n^{NL} accommodates all nonlinear processes. The control input to the nth mode can be written as

$$U_n(t) = \frac{\bar{a}^2}{\bar{p}E_n^2}\sum_{i=1}^{M}u_i(t)\psi_n(r_i) \tag{17}$$

where E_n denotes the Euclidean norm of the mode function.

To complete the formulation, we assume that the unsteady pressure field is monitored by P point sensors. Thus, the output signal measured at the position r_j in the chamber has the following form:

$$y_j(t) = c_j p'(r_j,t), \qquad j = 1, 2, \ldots, P \tag{18}$$

where c_j is a fixed real number, corresponding to the amplification factor of the pressure signal. The sensor output equation is found by substituting Eq. (13a) into Eq. (18), with the measurement noise modeled by a random function $v_j(t)$:

$$y_j(t) = c_j\bar{p}\sum_{n=1}^{K}\eta_n(t)\psi_n(r_j) + v_j(t), \qquad j = 1,2,\ldots,P \tag{19}$$

The system, Eqs. (16) and (19), can be described as stochastic, nonlinear, and multidimensional. We treat here only the deterministic and linear behavior of the system, i.e., $w_n(t) = v_j(t) = 0$ and $F_n^{NL} = 0$. Problems involving nonlinearities are addressed in Refs. 12 and 13.

Construction of State-Feedback Control

In this section, a digital control system based on the state-feedback technique is developed. The goal is to determine the control input $U_n(t)$ in such a way that the amplitude of pressure oscillation $\eta_n(t)$ can be controlled within a desired range as $t\to\infty$. As discussed with Eqs. (13), the oscillatory behavior of the combustion chamber is described by K modes. Realistically, however, it may not be practical to control all of these modes, since the actuators and sensors may not excite or respond to high-frequency oscillations because of hardware limitations. In addition, the onboard computational burden and model errors may restrict the control to a few critical modes. If only the first N modes are controlled with $N<K$, the state variables (defined here as the time-varying amplitudes of acoustic modes and their time derivatives) can be partitioned into controlled and uncontrolled (residual) parts as follows:

$$x = [x_N, x_R]^T \tag{20}$$

where

$$x_N = [\eta_1, \dot{\eta}_1, \ldots, \eta_N, \dot{\eta}_N]^T$$

$$x_R = [\eta_{N+1}, \dot{\eta}_{N+1}, \ldots, \eta_K, \dot{\eta}_K]^T$$

Thus, from Eqs. (16) and (19), the state-space and output equations can be written in the following vector form:

$$\dot{x}_N(t) = A_N x_N(t) + A_{NR} x_R(t) + B_N u(t) \tag{21a}$$

$$\dot{x}_R(t) = A_R x_R(t) + A_{RN} x_N(t) + B_R u(t) \tag{21b}$$

$$y(t) = C_N x_N(t) + C_R x_R(t) \tag{22}$$

where A_N, A_{NR} and A_R, A_{RN} are system-parameter matrices associated with the controlled and residual modes. Control input and sensor output matrices are represented by B_N, B_R and C_N, C_R, respectively, with their entries determined by the actuator and sensor positions. The control input and sensor output vectors are defined as

$$u(t) = [u_1(t), u_2(t), \ldots, u_M(t)]^T \tag{23}$$

$$y(t) = [y_1(t), y_2(t), \ldots, y_P(t)]^T \tag{24}$$

Because of the advantages of working with a modern digital computer, it is more convenient to implement the control system in the discrete-time domain than in the continuous-time domain. With the output signals measured at discrete sampling times, the system and output state-space equations in discrete time can be written as

$$x_N(k+1) = F_N x_N(k) + F_{NR} x_R(k) + G_N u(k) \tag{25a}$$

$$x_R(k+1) = F_R x_R(k) + F_{RN} x_N(k) + G_R u(k) \tag{25b}$$

$$y(k) = C_N x_N(k) + C_R x_R(k) \tag{26}$$

where F and G are

$$F = \exp(AT_S) \tag{27a}$$

$$G = \left[\int_0^{T_S} \exp(At')\, dt'\right] B \tag{27b}$$

and T_S is the sampling period. The functions $x(k)$ and $y(k)$ stand for the system states and outputs at the kth sampling instant ($t = kT_S$). An efficient algorithm for conversion of a discrete-time system from its counterpart in continuous time is given in Ref. 14.

Controller Design

The active controller must achieve the following two major functions: 1) determination of the control input $u(k)$ so that the amplitude of the pressure oscillation $\eta_n(k)$ will approach zero as $k \to \infty$; and 2) accommodation of a state estimator that receives the sensor measurement $y(k)$ and calculates an estimate of the state, $\hat{x}_N(k)$.

For a state-feedback system, the control law is simply the linear multiplication of the current state vector by a constant control gain matrix and the feedback of the result to the system. Since states are in general not directly available, the control input is based on the estimated state, giving

$$u(k) = -\mathcal{K}\hat{x}_N(k) \tag{28}$$

Thus, the controller design comes down to selecting an appropriate feedback gain matrix $\mathcal{K}$ that ensures system stability.

In this study, a Luenberger observer[15] is employed to estimate the system states in accordance with the sensor measurement and the control input, as shown in Fig. 2. It has the mathematical form

$$\hat{x}_N(k+1) = F_N \hat{x}_N(k) + G_N u(k) + \mathcal{L}[y(k) - C_N \hat{x}_N(k)] \tag{29}$$

where $\mathcal{L}$ is the observer gain matrix. Now define the estimation error vector $e_N(k)$ as

$$e_N(k) = x_N(k) - \hat{x}_N(k) \tag{30}$$

Substitution of Eqs. (25a), (26), and (29) into Eq. (30) yields

$$e_N(k+1) = (F_N - \mathcal{L}C_N)e_N(k) + (F_{NR} - \mathcal{L}C_R)x_R(k) \tag{31}$$

Finally, combining Eqs. (25b), (28), (30), and (31) and rearranging the result gives three coupled equations that describe the overall system behavior:

$$x_N(k+1) = (F_N - G_N\mathcal{K})x_N(k) + (G_N\mathcal{K})e_N(k) + F_{NR}x_R(k) \tag{32}$$

$$e_N(k+1) = (F_N - \mathcal{L}C_N)e_N(k) + (F_{NR} - \mathcal{L}C_R)x_R(k) \tag{33}$$

$$x_R(k+1) = (F_{RN} - G_R\mathcal{K})x_N(k) + (G_R\mathcal{K})e_N(k) + F_R x_R(k) \tag{34}$$

They can be conveniently recast to the matrix form:

$$\begin{bmatrix} x_N(k+1) \\ e_N(k+1) \\ x_R(k+1) \end{bmatrix} = \begin{bmatrix} F_N - G_N\mathcal{K} & G_N\mathcal{K} & F_{NR} \\ 0 & F_N - \mathcal{L}C_N & F_{NR} - \mathcal{L}C_R \\ F_{RN} - G_R\mathcal{K} & G_R\mathcal{K} & F_R \end{bmatrix} \times \begin{bmatrix} x_N(k) \\ e_N(k) \\ x_R(k) \end{bmatrix} \tag{35}$$

Obviously, in order to ensure system stability and accuracy of state estimation, the eigenvalues of Eq. (35) must be located inside the unit circle in the z plane.

For many practical propulsion devices involving distributed combustion, the influence of linear coupling terms on the system behavior appears to be quite weak,[16,17] since they represent fast-varying oscillations and vanish after appropriate time-averaging of the equations of motion. Almost identical results are obtained for linear stability characteristics no matter when the acoustic modes are treated simultaneously or independently. Therefore, to first approximation, we may ignore the coupling between controlled and residual modes in designing an active controller. Furthermore, the contribution of residual modes C_R in the sensor measurement can be either filtered out through a comb filter[18] or minimized by a judicious choice of sensor positions. With F_{NR}, F_{RN}, and C_R set to be zero, the system of Eq. (35) can be simplified as

$$\begin{bmatrix} x_N(k+1) \\ e_N(k+1) \\ x_R(k+1) \end{bmatrix} = \begin{bmatrix} F_N - G_N\mathcal{K} & G_N\mathcal{K} & 0 \\ 0 & F_N - \mathcal{L}C_N & 0 \\ -G_R\mathcal{K} & G_R\mathcal{K} & F_R \end{bmatrix} \begin{bmatrix} x_N(k) \\ e_N(k) \\ x_R(k) \end{bmatrix} \tag{36}$$

The characteristic equation of the system of Eq. (36) is

$$\det[zI - F_N + G_N\mathcal{K}] \cdot \det[zI - F_N + \mathcal{L}C_N] \cdot \det[zI - F_R] = 0 \tag{37}$$

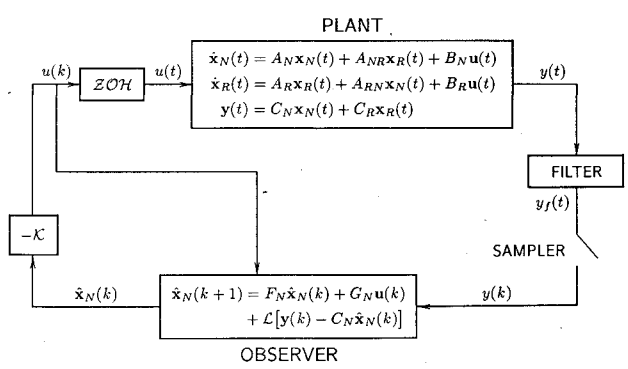

Fig. 2 Structure of the digital control system.

Equation (36) can be regarded as a small variation from the actual system, with its eigenvalues determined by the individual matrices $(F_N - G_N\mathcal{K})$, $(F_N - \mathcal{L}C_N)$, and F_R. Since the uncoupled residual modes are usually stable, the matrices $\mathcal{K}$ and $\mathcal{L}$ must be chosen to have the eigenvalues of $(F_N - G_N\mathcal{K})$ and $(F_N - \mathcal{L}C_N)$ located inside the unit circle in the z plane for stability. Hence, it is straightforward to guarantee the stability of the system, Eq. (36), by a suitable controller design. The structure of Eq. (36) also leads to the well-known separation principle that implies that $\mathcal{K}$ and $\mathcal{L}$ can be determined separately.

Owing to the great simplicity of the separation principle and the relatively less significance of the off-diagonal terms in the model Eq. (16) and of the elements of C_R, it is proposed to first design the controller according to the approximated system, Eq. (36), and then implement the controller into the original system, Eq. (35). Finally, the validity of this approach will be corroborated by direct examination of the stability of the actual system.

Determination of Control and Observer Gain Matrices

For a closed-loop system, the controller and observer characteristic equations can be written respectively as

$$\det[zI - F_N + G_N\mathcal{K}] = z^{2N} + \bar{\alpha}_1 z^{2N-1} + \cdots + \bar{\alpha}_{2N} \tag{38}$$

$$\det[zI - F_N + \mathcal{L}C_N] = z^{2N} + \bar{\beta}_1 z^{2N-1} + \cdots + \bar{\beta}_{2N} \tag{39}$$

with coefficients $\bar{\alpha}_i$ and $\bar{\beta}_i$ determined by desired eigenvalues of the matrices $(F_N - G_N\mathcal{K})$ and $(F_N - \mathcal{L}C_N)$.

To ensure system stability and accuracy of state estimation, the gain matrices $\mathcal{K}$ and $\mathcal{L}$ must be determined in such a way that the eigenvalues of $(F_N - G_N\mathcal{K})$ and $(F_N - \mathcal{L}C_N)$ are located inside the unit circle in the z plane, provided conditions for controllability and observability are fulfilled.[14] This requires the following controllability and observability matrices to be nonsingular:

$$\mathcal{C} = [G_N \quad F_N G_N \quad F_N^2 G_N \cdots F_N^{2N-1} G_N] \tag{40}$$

$$\mathcal{O} = \begin{bmatrix} C_N \\ C_N F_N \\ C_N F_N^2 \\ \vdots \\ C_N F_N^{2N-1} \end{bmatrix} \tag{41}$$

For problems involving only a single input and a single output, the controller and observer gain vectors can be evaluated according to Ackermann's formula[19]:

$$\mathcal{K} = [0 \cdots 0 \quad 1]\,[\mathcal{C}]^{-1}\mathcal{A}(F_N) \tag{42}$$

$$\mathcal{L} = \mathcal{B}(F_N)\,[\mathcal{O}]^{-1}\begin{bmatrix} 0 \\ \vdots \\ 0 \\ 1 \end{bmatrix} \tag{43}$$

where

$$\mathcal{A}(F_N) = F_N^{2N} + \bar{\alpha}_1 F_N^{2N-1} + \cdots + \bar{\alpha}_{2N} I$$

$$\mathcal{B}(F_N) = F_N^{2N} + \bar{\beta}_1 F_N^{2N-1} + \cdots + \bar{\beta}_{2N} I$$

For multiple inputs and outputs, algorithms are available to determine $\mathcal{K}$ and $\mathcal{L}$.[20] In general, the closed-loop system poles are chosen so that the pressure oscillations can be suppressed effectively with a minimum possible amount of energy used for the control input. The observer poles are then specified for a somewhat faster decay rate for the estimated error (approximately a factor of four), so that the estimated states will approach true states in a relatively short time, and the dynamics of the closed-loop system will be governed primarily by the controller poles.

Locations of Actuator and Sensor

The locations of actuators must be selected carefully because of their direct influence on the effectiveness of control actions. For longitudinal oscillations, the coefficient of an input for the nth mode is proportional to $\psi_n(z_a)$, in which z_a stands for the actuator position. If the forcing is exerted at a pressure nodal point at which the function ψ_n vanishes, obviously it cannot modify the nth mode of the flowfield. Therefore, the coefficient of each input in Eq. (17) should be as large as possible for the controlled modes to enhance the system controllability.

On the other hand, the input signal that drives the controlled states to zero may also excite the residual modes, a phenomenon commonly known as control spillover. Thus, the coefficient of each input for the residual modes must be minimized to circumvent this problem. In order to increase system controllability and alleviate control spillover, the actuator location z_a is chosen to minimize the following objective function:

$$J = W_N \sum_{n=1}^{N} [1 - |\psi_n(z_a)|]^2 + W_R \sum_{n=N+1}^{K} [\psi_n(z_a)]^2 \tag{44}$$

where W_N and W_R are the weighting factors for the controlled and residual modes, respectively. Figure 3 shows the dependence of the objective function J on the actuator location z_a, with only two controlled and two residual modes taken into account. If the influence of the residual modes is ignored (i.e.,

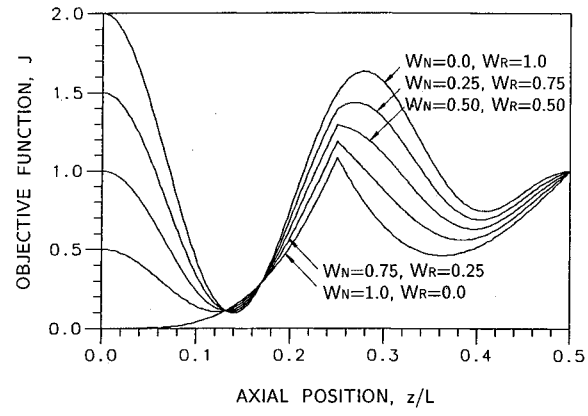

Fig. 3 Objective function for selection of actuator and sensor locations (two controlled and two residual modes).

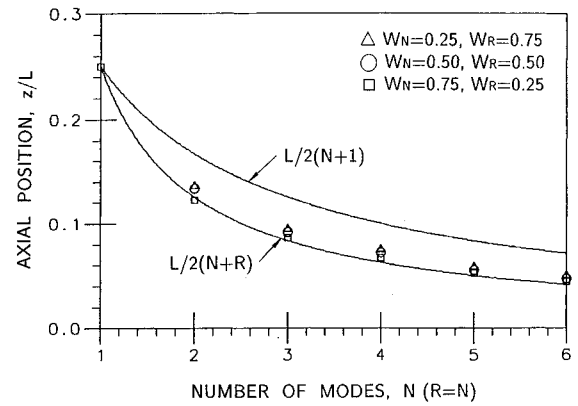

Fig. 4 Optimal locations of sensors and actuators for various numbers of modes ($N = R$).

$W_R = 0$), the most effective position for the actuator is the head end of the chamber and $J = 0$ at that point. However, this location may give rise to a severe control spillover problem. For nonzero values of W_R in Fig. 3, the optimal actuator location falls between the first nodal points of the lowest and highest residual modes, i.e., $L/(2N + 2R) < z_a < L/(2N + 2)$. Figure 4 shows the optimal actuator locations for various controlled and residual modes, in which $N = R$. The result matches closely the curve $z_a = L/(2N + 2R)$.

Equation (19) also suggests that the minimization of Eq. (44) leads to an increase in the value of each element of C_N and a reduction in that of C_R. This implies that the system observability for the controlled modes will be enhanced and the observation spillover problem reduced. The optimal sensor location is accordingly selected to be the same as the actuator location.

Illustrative Examples and Discussions

The state-feedback control algorithm described in the preceding sections can be implemented effectively to suppress undesired thermal-acoustic instabilities in combustion chambers. To demonstrate its performance, a series of numerical simulations were conducted for systems with distributed combustion. The unsteady combustion process was modeled using a linear pressure-coupled response function. As an example, we consider here the problem involving two controlled and two residual modes of longitudinal oscillations. The normalized natural radian frequency of the fundamental mode is taken to be unity, and the linear parameters D_{ni} and E_{ni} in Eq. (16) are given in Table 1.

These coefficients are representative of a typical situation observed in many practical combustion devices such as rocket motors.[12] The overall open-loop system eigenvalues in both continuous and discrete time are summarized in Table 2, in which each pole represents the corresponding eigenvalue of that mode. Note that the first mode is linearly unstable with a growth constant of 0.005, and the second mode is linearly stable with a decay coefficient 10 times larger than that of the first mode.

The controller design is based on the dynamics of the controlled modes only, i.e., on the basis of Eqs. (25a) and (26), with F_{NR} and C_R taken to be zero. In addition, only one set of sensor and actuator is used to estimate the states and subsequently provide the stabilizing control input. The design procedure involves four steps. First, the actuator and sensor locations are selected to be at $z_a = L/7.5$ in accordance with Figs. 3 and 4, with no amplification of the measured pressure signal. Second, the sampling period is set at 1% of the period of the fundamental mode, i.e., $T_S = 0.01$. For this sampling period, it has been verified by evaluating the determinants of the matrices $\mathcal{C}$ and $\mathcal{O}$ that the system is observable and controllable. With only the first four modes included in the analysis, it also satisfies the Nyquist sampling criterion.[14] Third, the feedback gain matrix $\mathcal{K}$ is chosen by placing the closed-loop poles inside the unit circle in the z plane. In general, the higher the distance between the open-loop and closed-loop

Table 1 System parameters

D_{ni}	$i=1$	$i=2$	$i=3$	$i=4$
$n=1$	−0.01	0.007	−0.001	0.007
$n=2$	0.01	0.1	0.007	−0.001
$n=3$	−0.01	0.01	0.75	0.008
$n=4$	0.02	−0.005	0.01	1.50
E_{ni}	$i=1$	$i=2$	$i=3$	$i=4$
$n=1$	−0.005	−0.005	0.0025	0.0016
$n=2$	−0.0025	−0.015	0.01	0.01
$n=3$	−0.005	0.0	−0.02	0.02
$n=4$	0.01	0.02	0.02	−0.025

Table 2 Open-loop system poles

	Continuous time	Discrete time
Mode 1	$0.00499 \pm j0.99750$	$1.00005 \pm j0.00998$
Mode 2	$-0.04998 \pm j1.99560$	$0.99950 \pm j0.01996$
Mode 3	$-0.37499 \pm j2.97309$	$0.99625 \pm j0.02973$
Mode 4	$-0.75003 \pm j3.92585$	$0.99216 \pm j0.03904$

Table 3a Closed-loop system poles (case 1)

	Approximated[a]	Actual[b]
Pole 1	$0.99985 \pm j0.00997$	$0.99985 \pm j0.00997$
Pole 2	$0.99950 \pm j0.01996$	$0.99950 \pm j0.01996$
Pole 3	$0.99625 \pm j0.02973$	$0.99625 \pm j0.02973$
Pole 4	$0.99216 \pm j0.03904$	$0.99216 \pm j0.03904$
Pole 5	$0.99804 \pm j0.00397$	$0.99804 \pm j0.00397$
Pole 6	$0.99700 \pm j0.00208$	$0.99700 \pm j0.00208$

[a]Based on the separation principle, Eq. (36).
[b]Based on the complete system, Eq. (35).

Table 3b Closed-loop system poles (case 2)

	Approximated[a]	Actual[b]
Pole 1	$0.99955 \pm j0.00997$	$0.99955 \pm j0.00997$
Pole 2	$0.99950 \pm j0.01996$	$0.99950 \pm j0.01996$
Pole 3	$0.99625 \pm j0.02973$	$0.99625 \pm j0.02973$
Pole 4	$0.99216 \pm j0.03904$	$0.99216 \pm j0.03904$
Pole 5	$0.99804 \pm j0.00397$	$0.99804 \pm j0.00397$
Pole 6	$0.99700 \pm j0.00208$	$0.99700 \pm j0.00208$

[a]Based on the separation principle, Eq. (36).
[b]Based on the complete system, Eq. (35).

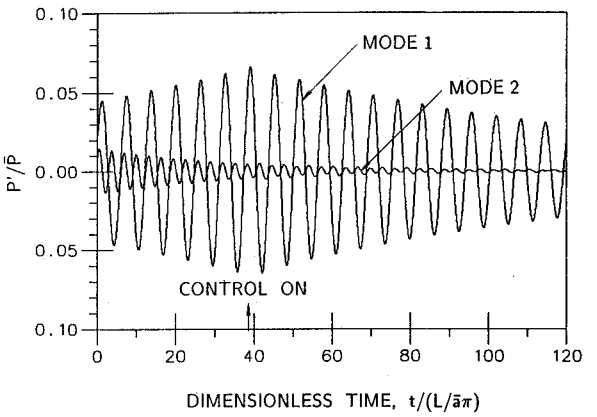

Fig. 5 Time traces of oscillations of controlled modes at the chamber head end for case 1 ($\omega_1 = 1$, $\omega_2 = 2$).

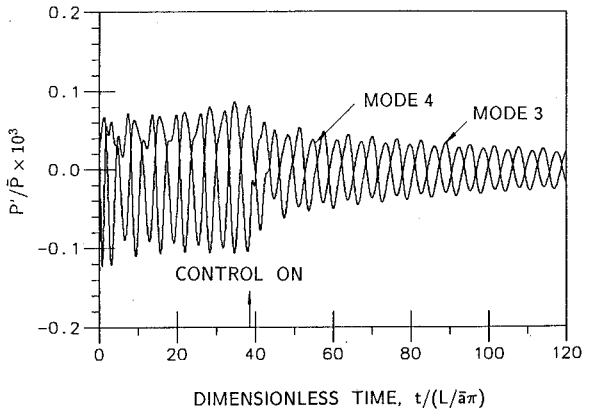

Fig. 6 Time traces of oscillations of residual modes at the chamber head end for case 1 ($\omega_3 = 3$, $\omega_4 = 4$).

poles, the greater the required control input energy. Therefore, the stable open-loop poles remain unchanged, and the unstable poles are relocated slightly inside the unit circle by moving them radially toward the origin of the z plane. Finally, in order to provide a good overall system performance, the observer poles are taken to have a decay rate for the estimation error about four times faster than that for the controlled modes.[14]

Two controller designs, case 1 and case 2, were carried out, with the unstable open-loop poles relocated to positions having radii of 0.9999 and 0.9996 in the z plane, respectively (see Table 3, where poles 5 and 6 are associated with the estimation errors for modes 1 and 2, respectively). Because the observation spillover and the linear coupling between the controlled and residual modes were ignored in the controller design, the eigenvalues based on the approximated system, Eq. (36), were expected to be slightly different from those of the actual system, Eq. (35). However, the deviation is quite small, and has little influence on the entire system performance. For this particular case, these eigenvalues are exactly the same within five digits. Figure 5 shows the calculated time histories of the controlled modes for case 1. A small initial disturbance grows exponentially for some time until its amplitude reaches a preset threshold value at which the controller is activated to suppress oscillations. The system functions quite effectively, and eliminates undesired oscillations within a few cycles. Figure 6 shows the time traces of oscillations of residual modes. High-frequency disturbances are initiated at $t = 0$ due to the coupling with controlled modes, and then decay rapidly when the system becomes stable. The estimation error e_N was also calculated, giving the results shown in Fig. 7. The observer is capable of estimating the states closely, except during the short starting transient period due to errors associated with estimation of initial states.

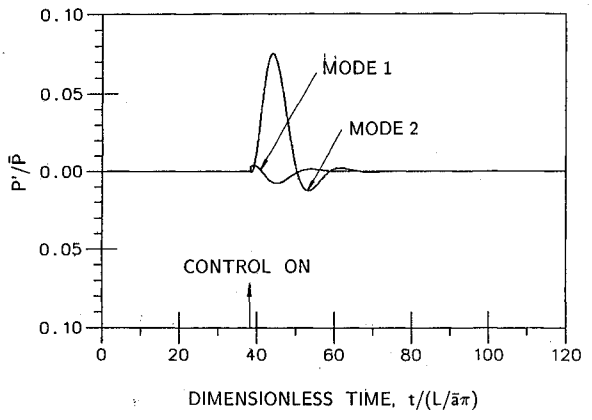

Fig. 7 Time traces of estimation errors for case 1.

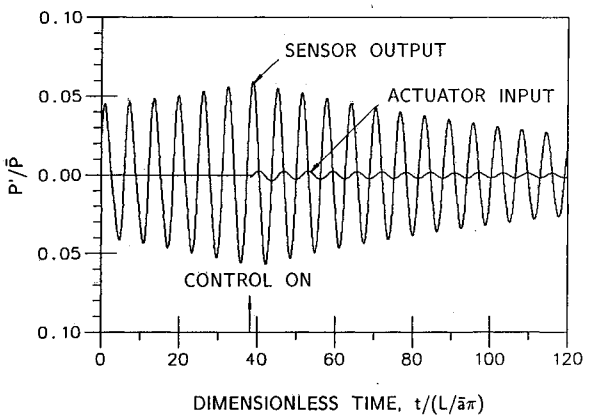

Fig. 8 Time traces of the control input $u(t)$ and sensor output $y(t)$ for case 1.

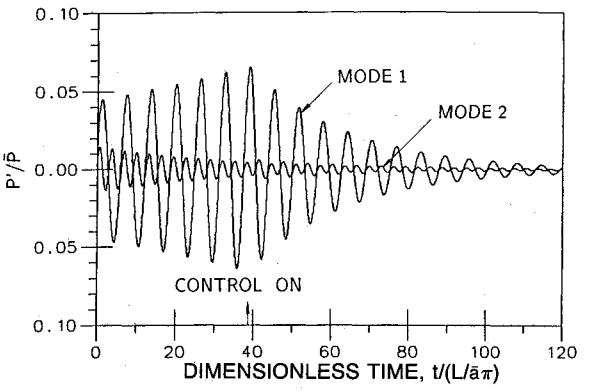

Fig. 9 Time traces of oscillations of controlled modes at the chamber head end for case 2 ($\omega_1 = 1$, $\omega_2 = 2$).

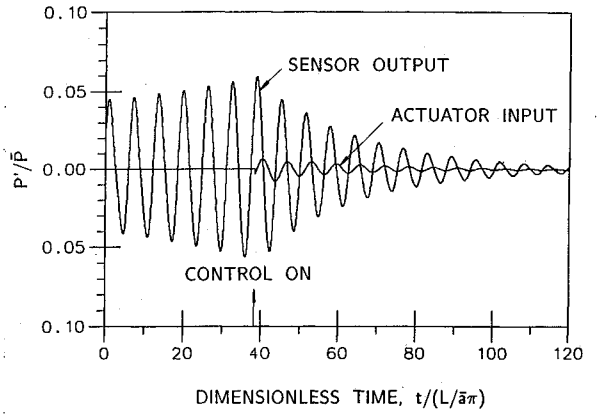

Fig. 10 Time trace of the control input $u(t)$ and sensor output $y(t)$ for case 2.

One of the fundamental issues in the design of an active control system is the tradeoff between the energy of unsteady motions and the energy required to eliminate them. To see this, the input pressure $u(t)$ at the actuator location was calculated. Figure 8 indicates that the system needs only a small amount of energy in the initial stage to control the oscillations. The maximum input pressure that occurred immediately after the actuation of the controller is less than 5% of the maximum pressure oscillation.

As discussed previously, the closed-loop pole locations affect significantly the overall system characteristics. Their influence on the controller performance appears usually in two aspects: the amplitude of control inputs, and the time duration required to suppress oscillations. In general, a decrease in the magnitude of the closed-loop poles reduces the control duration but increases the maximum amplitude of the control input. This means that a faster decay of oscillation is associated with a higher demand for control input. For the purpose of illustration, simulation results are also presented for case 2, in which the unstable open-loop poles are shifted to a radial position of 0.9996 from the origin in the z plane. Figures 9 and 10 show the calculated time traces of the controlled oscillations and the input pressure, respectively. Compared with case 1, the actuator can indeed eliminate disturbance within a much shorter interval (i.e., 15 cycles in this example), but the maximum amplitude of the pressure input increases from 5 to 12% of the threshold value. Since these are the amplitude and response times of the control inputs, and to a much lesser extent the control duration, which limit the applicability of an active controller in practical combustion systems, the unstable open-loop poles should be relocated as close to the unit circle in the z plane as possible.

Concluding Remarks

A linear theory has been developed to study the active control of longitudinal pressure oscillations in a combustion

chamber. The control actions were provided by a number of point actuators, with the state of the system measured at a few representative locations. As a specific example, the case involving two controlled and two residual modes was studied in depth. The control and observation spillover phenomena induced by the motions of residual modes were clearly demonstrated.

Although this work offers a formal treatment of the state-feedback control of combustion instabilities, several aspects require extensive attention in the future. First, the system parameters of each oscillatory mode were treated as known quantities in advance. For many practical combustion systems involving complex physicochemical processes, these parameters may not be determined accurately and economically. Therefore, a design using an adaptive controller that can learn and improve its performance as it operates may provide a realistic solution. Second, we have dealt only with the linear control of longitudinal pressure oscillations. Extension to nonlinear analysis is required in order for many important nonlinear phenomena (e.g., triggering of oscillations and limit cycles) to be studied. Third, the present model assumes time-invariant mean flowfields and employs a modal expansion of oscillatory fields. Thus, it excludes the existence of hydrodynamic instabilities, in particular shear layer and vortical instabilities. Extension should be made to accommodate all three classes of unsteady flow motions: acoustic, entropy, and vortical modes. This is likely a key issue in the entire problem. Consequently, a more realistic and complete representation of actual systems can be achieved.

References

[1]Harrje, D. T., and Reardon, F. H., (eds.), *Liquid-Propellant Rocket Combustor Instability,* NASA SP-194, 1972.

[2]Dine, P. J., "Active Control of Flame Noises," Ph.D. Dissertation, Cambridge Univ., Cambridge, England, UK, 1983.

[3]Heckl, M. A., "Heat Sources in Acoustic Resonators," Ph.D. Dissertation, Cambridge Univ., Cambridge, England, UK, 1985.

[4]Sreenivasan, K. R., Raghu, S., and Chu, B. T., "The Control of Pressure Oscillations in Combustion and Fluid Dynamical System," AIAA Paper 85-0544, March 1985.

[5]Bloxsidge, G. J., Dowling, A. P., Hooper, N., and Langhorne, P. J., "Active Control of an Acoustically Driven Combustion Instability," *Journal of Theoretical and Applied Mechanics,* Vol. 6, 1987, pp. 161–175.

[6]Lang, W., Poinsot, T., and Candel, S., "Active Control of Combustion Instability," *Combustion and Flame,* Vol. 70, 1987, pp. 281–289.

[7]Poinsot, T., Bourienne, F., Candel, S., Esposito, E., and Lang, W., "Suppression of Combustion Instabilities by Active Control," *Journal of Propulsion and Power,* Vol. 5, No. 1, 1987, pp. 14–20.

[8]Poinsot, T., Veynante, D., Bourienne, F., Candel, S., Esposito, E., and Surget, J., "Initiation and Suppression of Combustion Instabilities by Active Control," *Proceedings of the 22nd Symposium (International) on Combustion,* The Combustion Inst., Pittsburgh, PA, 1988, pp. 1363–1370.

[9]Culick, F. E. C., "Nonlinear Behavior of Acoustic Waves in Combustion Chambers," *Acta Astronautica,* Vol. 3, 1976, pp. 715–756.

[10]Culick, F. E. C., and Yang, V., "Prediction of the Stability of Unsteady Motions in Solid Propellant Rocket Motors," to appear in *Nonsteady Burning and Combustion Stability of Solid Propellants,* edited by L. DeLuca and M. Summerfield, Progress in Astronautics and Aeronautics, AIAA, Washington, DC, 1991.

[11]Fung, Y. T., Yang, V., and Sinha A., "Active Control of Combustion Instabilities with Distributed Actuators," *Combustion Science and Technology* (to be published).

[12]Fung, Y. T., "Active Control of Linear and Nonlinear Pressure Oscillations in Combustion Chambers," Ph.D. Dissertation, Pennsylvania State Univ., University Park, PA, 1991.

[13]Yang, V., and Fung, Y. T., "Active Control of Nonlinear Pressure Oscillations in Combustion Chambers," AIAA Paper 91-2079, June 1991.

[14]Franklin, G. F., and Powell, J. D., *Digital Control of Dynamic System,* Addison-Wesley, Reading, MA, 1980.

[15]Luenberger, D. G., "An Introduction to Observers," *IEEE Transactions on Automatic Control,* Vol. AC-16, 1971, pp. 596-602.

[16]Zinn, B. T., and Lores, M. E., "Application of the Galerkin Method in the Solution of Nonlinear Axial Combustion Instability Problems in Liquid Rockets," *Combustion Science and Technology,* Vol. 4, 1972, pp. 269–278.

[17]Yang, V., and Culick, F. E. C., "On the Existence and Stability of Limit Cycles for Transverse Acoustic Modes in a Combustion Chamber," *Combustion Science and Technology,* Vol. 72, 1990, pp. 37–65.

[18]Balas, M. J., "Feedback Control of Flexible Systems," *IEEE Transactions on Automatic Control,* Vol. AC-23, No. 4, 1978, pp. 673–679.

[19]Ogata, K., *Discrete-Time Control System,* Prentice-Hall, Englewood Cliffs, NJ, 1987.

[20]Kailath, T., *Linear System,* Prentice-Hall, Englewood Cliffs, NJ, 1980.